Some Effects of an Elliptic Ridge on Waves of Tidal Frequency[1]

RICHARD W. REYNOLDS[2]

Department of Oceanography, University of Hawaii, Honolulu, 96822

(Manuscript received 21 May 1976, in final form 10 October 1977)

ABSTRACT

A numerical finite-difference model using the Laplace tidal equations on an f-plane was developed to predict how tidal motion is disturbed by an elliptic ridge. With the use of an open-ocean matching condition the model was used to study the effects of several generalized types of elliptic bottom topographies and to study the particular case of the Hawaiian Ridge.

1. Introduction

Reviews of recent tidal literature by Hendershott and Munk (1970) and Hendershott (1973) discussed a great variety of global numerical models of ocean tides. In these models, one of the most prominent of the topographical features of the Pacific Ocean, the Hawaiian Ridge, is so narrow that it was completely lost in the smoothing operations. However, both Luther and Wunsch (1975) and Larsen (1977) have observed considerable phase differences between tidal stations on opposite sides of the eastern end of the Hawaiian Ridge.

In response to this problem, an open-ocean numerical model with a long elliptic ridge was developed. Assuming that tides can be approximated locally as independent free waves, this model was used in an attempt to explain tidal elevations throughout the Hawaiian Ridge.

2. Differential equation and inner boundary conditions

The problem was formulated in elliptical cylindrical coordinates (μ, ϕ), defined in terms of Cartesian coordinates (x, y) as

$$\left.\begin{aligned} x &= \tfrac{1}{2}a \cosh\mu \cos\phi \\ y &= \tfrac{1}{2}a \sinh\mu \sin\phi \end{aligned}\right\}, \qquad (1)$$

where a is the distance between the foci of the coordinate system, $0 \leq \phi < 2\pi$ and $\mu \geq 0$.

In this coordinate system, the Laplace equations for a periodic barotropic tide with constant rotation and without forcing terms were given by Platzman (1971) as

$$L(Z) = \frac{\partial}{\partial\mu}\left(h\frac{\partial Z}{\partial\mu}\right) + \frac{\partial}{\partial\phi}\left(h\frac{\partial Z}{\partial\phi}\right) + \frac{if}{\sigma}\left(\frac{\partial h}{\partial\mu}\frac{\partial Z}{\partial\phi} - \frac{\partial h}{\partial\phi}\frac{\partial Z}{\partial\mu}\right) + \alpha^2\left(\frac{\sigma^2 - f^2}{g}\right)Z = 0. \qquad (2)$$

Here $Z(\mu,\phi)$ is the time-independent sea surface elevation, defined in terms of the time-dependent sea surface elevation ζ by $\zeta(\mu,\phi,t) = \mathrm{Re}[Z(\mu,\phi)\exp(-i\sigma t)]$, where σ is the time harmonic frequency of the motion and t time. The remaining quantities are as follows:

$L(Z)$	the differential operator on Z
$h(\mu,\phi)$	the undisturbed water depth
f	the Coriolis parameter
g	the acceleration of gravity

and

$$\alpha = \tfrac{1}{2}a(\sinh^2\mu + \sin^2\phi)^{1/2}.$$

In the simple case of constant depth h_0, Eq. (2) reduces to the Helmholtz equation

$$L^0(Z) = \frac{\partial^2 Z}{\partial\mu^2} + \frac{\partial^2 Z}{\partial\phi^2} + \alpha^2 K^2 Z = 0, \qquad (3)$$

where

$$K = \left(\frac{\sigma^2 - f^2}{gh_0}\right)^{1/2}$$

and $L^0(Z)$ is the operator L when $h = h_0$.

The inner boundary condition was formulated by requiring no normal flow through a vertical wall boundary. This condition can be expressed in terms of Z as

$$\frac{\partial Z}{\partial n} + \frac{if}{\sigma}\frac{\partial Z}{\partial s} = 0, \qquad (4)$$

[1] Hawaii Institute of Geophysics Contribution No. 856.

[2] Present affiliation: Climatic Research Institute, Oregon State University, Corvallis 97331.

0022-3670/78/0038-0046$05.00

© 1978 American Meteorological Society

Unauthenticated | Downloaded 10/11/24 11:03 AM UTC

where n is directed normally outward from the boundary and s is directed along the tangent in a direction counterclockwise from n.

3. Incoming and scattered waves

The solution was determined for an infinite ocean, which was split into a constant depth $h = h_0$, an exterior region where $\mu \geq \mu_0$, and an interior region $\mu \leq \mu_0$ with variable depth and possible islands. The sea surface elevation Z was also split into a known incoming wave Z_0 and a scattered wave Z_s, where $Z = Z_0 + Z_s$. The incoming wave was assumed to satisfy (3), i.e.,

$$L^0(Z_0) = 0, \tag{5}$$

in both the interior and exterior regions.

The scattered wave is the sea surface elevation disturbance which results when Z_0, in the interior region, is perturbed by the topography in that region. The differental and inner boundary equation for $Z_s = Z_s^I$ follow from (2), (4) and (5):

$$L(Z_s^I) = -L(Z_0), \tag{6}$$

$$\frac{\partial Z_s^I}{\partial n} + \frac{if}{\sigma}\frac{\partial Z_s}{\partial s} = -\frac{\partial Z_0}{\partial n} - \frac{if}{\sigma}\frac{\partial Z_0}{\partial s}. \tag{7}$$

In the exterior region the scattered wave $Z_s = Z_s^x$ satisfies (3), i.e.,

$$L^0(Z_s^x) = 0. \tag{8}$$

The matching condition for Z_s at the transition between the interior and exterior region and the boundary condition for Z_s at infinity are discussed in the following section.

4. Matching and outer boundary conditions

The solution Z_s^I can be solved numerically in the interior region if a matching condition can be found for Z_s^I and Z_s^x at $\mu = \mu_0$. This can be done by separating both (8) in the exterior region and (6) in the interior region at $\mu = \mu_0$ into two equations:

$$\Phi'' + (b - 2q\cos 2\phi)\Phi = 0, \tag{9}$$

$$\eta'' - (b - 2q\cosh 2\mu)\eta = 0, \tag{10}$$

where the prime indicates differentiation, b is a separation constant and

$$q = \frac{a^2}{16}K^2.$$

The solution to the Mathieu equation (9) must be periodic by definition of ϕ. Thus solutions exist only for a countably infinite set of eigenvalues. The eigensolutions $Se_m(\phi)$ and $So_m(\phi)$ are even and odd about $\phi = 0$, respectively. The corresponding eigenvalues are defined by be_m ($m = 0, 1, 2, \ldots$) and bo_m ($m = 1, 2, 3, \ldots$). The eigenvalues differ ($be_m \neq bo_m$) except in the degenerate case $a = 0$, when the elliptical coordinates reduce to polar coordinates. The solutions satisfy the orthogonality relationships

$$\left.\begin{aligned} \int_0^{2\pi} Se_m(\phi)Se_n(\phi)d\phi &= Ne_m\delta_{mn} \\ \int_0^{2\pi} So_m(\phi)So_n(\phi)d\phi &= No_m\delta_{mn} \\ \int_0^{2\pi} So_m(\phi)Se_n(\phi)d\phi &= 0 \end{aligned}\right\}, \tag{11}$$

where m and n are integers, δ_{mn} is the Kronecker delta, and Ne_m and No_m are normalizing constants (Morse and Feshbach, 1953).

The solution to the modified Mathieu equation (10) can be expressed in terms of Bessel functions. For both even and odd solutions, there are two independent solutions made up of expressions of Bessel functions of the first kind J_m and the second kind Y_m (cf. Blanch, 1964). The set of even elliptic solutions are written as $Je_m(\mu)$ and $Ye_m(\mu)$; the odd set as $Jo_m(\mu)$ and $Yo_m(\mu)$. If $\eta e_m(\mu)$ and $\eta o_m(\mu)$ represent the linear combinations of Je, Ye and Jo, Yo, respectively, the scattered waves can be expressed as

$$Z_s^I(\mu_0,\phi) = \sum_{m=0}^{\infty} \eta e_m^I(\mu_0)Se_m(\phi) + \sum_{m=1}^{\infty} \eta o_m^I(\mu_0)So_m(\phi), \tag{12}$$

$$Z_s^x(\mu,\phi) = \sum_{m=0}^{\infty} \eta e_m^x(\mu)Se_m(\phi). + \sum_{m=1}^{\infty} \eta o_m^x(\mu)So_m(\phi). \tag{13}$$

The separation of variables allowed the definition of a ϕ independent admittance

$$\left.\begin{aligned} We_m(\mu) &= \eta' e_m(\mu)/\eta e_m(\mu) \\ Wo_m(\mu) &= \eta' o_m(\mu)/\eta o_m(\mu) \end{aligned}\right\}. \tag{14}$$

The requirement of the continuity of the admittances at $\mu = \mu_0$ resulted in a matching condition

$$\left.\begin{aligned} We_m^I(\mu_0) &= We_m^x(\mu_0) \\ Wo_m^I(\mu_0) &= Wo_m^x(\mu_0) \end{aligned}\right\}. \tag{15}$$

Before finding $We_m^x(\mu)$ and $Wo_m^x(\mu)$, $We_m^I(\mu_0)$ and $Wo_m^I(\mu_0)$ were expressed in terms of $Z_s^I(\mu_0,\phi)$. One method of doing this is to first apply the orthogonality expressions of (11) to (12) to yield

Unauthenticated | Downloaded 10/11/24 11:03 AM UTC

$$\left.\begin{aligned} \eta e_m^I &= \frac{1}{Ne_m}\int_0^{2\pi} Z_s^I(\mu_0,\tilde{\phi})\,Se_m(\tilde{\phi})\,d\tilde{\phi} \\ \eta o_m^I &= \frac{1}{No_m}\int_0^{2\pi} Z_s^I(\mu_0,\tilde{\phi})\,So_m(\tilde{\phi})\,d\tilde{\phi} \end{aligned}\right\}, \quad (16)$$

where $\tilde{\phi}$ is the dummy integration variable. Upon differentiating (12) with respect to μ at μ_0 and replacing $\eta e_m^{I\prime}(\mu_0)$ by $\eta e_m^I(\mu_0)We_m^I(\mu_0)$ and $\eta o_m^{I\prime}(\mu_0)$ by $\eta o_m^I(\mu_0)Wo_m^I(\mu_0)$ from the definition (14), $\eta e_m^I(\mu_0)$ and $\eta o_m^I(\mu_0)$ can be eliminated by (16) yielding

$$\begin{aligned} \frac{\partial Z_s^I(\mu_0,\phi)}{\partial\mu} &= \sum_{m=0}^{\infty}\frac{We_m^I(\mu_0)\,Se_m(\phi)}{Ne_m} \\ &\quad\times\int_0^{2\pi} Z_s^I(\mu_0,\phi)\,Se_m(\phi)\,d\phi \\ &\quad+\sum_{m=1}^{\infty}\frac{Wo_m^I(\mu_0)\,So_m(\phi)}{No_m} \\ &\quad\times\int_0^{2\pi} Z_s^I(\mu_0,\phi)\,So_m(\phi)\,d\phi. \end{aligned} \quad (17)$$

Although nothing new has been added, $Z_s^I(\mu_0,\phi)$ and its derivative have now been expressed locally at $\mu = \mu_0$ in terms of the admittances, We^I and Wo^I.

To find We_m^x and Wo_m^x, a Sommerfeld radiation condition was applied to (13). This boundary condition excludes any incoming energy at infinity and is appropriate for a scattered wave on an infinite ocean. For a two-dimensional problem with an $\exp(-i\sigma t)$ time-dependence, the condition (cf. Chester, 1971) is

$$\lim_{r\to\infty} r^{1/2}\left(\frac{\partial Z_s}{\partial r} - iKZ_s\right) = 0, \quad (18)$$

where $r = (x^2 + y^2)^{1/2}$. Reynolds (1975) substituted (13) into (18) and showed that $\eta e_m^x(\mu)$ and $\eta o_m^x(\mu)$ must be proportional to $He_m(\mu)$ and $Ho_m(\mu)$, respectively, where He and Ho are the elliptic Hankel functions defined as

$$\left.\begin{aligned} He_m(\mu) &= Je_m(\mu) + iYe_m(\mu) \\ Ho_m(\mu) &= Jo_m(\mu) + iYo_m(\mu) \end{aligned}\right\}.$$

Thus the admittances (14) must take the form

$$\left.\begin{aligned} We_m^x(\mu) &= He_m'(\mu)/He_m(\mu) \\ Wo_m^x(\mu) &= Ho_m'(\mu)/Ho_m(\mu) \end{aligned}\right\} \quad (19)$$

in the exterior region. [In Reynolds (1975) these admittances were also found independently by formal application of the transport method of Preisendorfer (1972).]

Eq. (19) allows the matching condition (15) to be expressed as

$$\left.\begin{aligned} We_m^I(\mu_0) &= We_m^x(\mu_0) = He_m'(\mu_0)/He_m(\mu_0) \\ Wo_m^I(\mu_0) &= Wo_m^x(\mu_0) = Ho_m'(\mu_0)/Ho_m(\mu_0) \end{aligned}\right\}. \quad (20)$$

With the use of (17), Eq. (20) can now be expressed in terms of $Z_s^I(\mu_0,\phi)$ which after rearranging gave

$$\begin{aligned} &\frac{\partial Z_s^I(\mu_0,\phi)}{\partial\mu} \\ &\quad-\int_0^{2\pi} Z_s^I(\mu_0,\tilde{\phi})\left\{\sum_{m=0}^{\infty}\frac{Se_m(\tilde{\phi})\,Se_m(\phi)}{Ne_m}\left[\frac{He_m'(\mu_0)}{He_m(\mu_0)}\right]\right. \\ &\quad\left.+\sum_{m=1}^{\infty}\frac{So_m(\tilde{\phi})\,So_m(\phi)}{No_m}\left[\frac{Ho_m'(\mu_0)}{Ho_m(\mu_0)}\right]\right\}d\tilde{\phi} = 0. \end{aligned} \quad (21)$$

Eq. (21) is the desired condition for Z_s^I on the outer boundary of the interior region. It can be used with the differential equation (6) and the inner boundary equation (7) to define $Z_s^I(\mu,\phi)$ within the interior region.

It is important to recall that (21) was determined from a matching condition with the external admittances given by (19). These admittances are valid only for free scattered waves which satisfy the radiation condition in the infinite flat-bottomed f-plane, exterior region.

5. The numerical solution

Now that the basic differential and boundary equations have been specified, the system of equations may be solved numerically for the scattered wave in the interior region. To begin, a regular elliptic grid was constructed such that

$$\begin{aligned} &\mu = k\Delta\mu, \quad \text{where } k = 0, 1, \ldots, M, \\ &\phi = l\Delta\phi, \quad \text{where } l = 0, 1, \ldots, N-1, \\ &\qquad \text{and} \quad \text{where } \Delta\phi = 360°/N. \end{aligned}$$

Using this grid, the inner boundary equation (7) and the differential equation (6) were changed by replacing the derivatives of Z_s (where the superscript I can henceforth be dropped) by a finite-difference approximation. Either the finite version of (7) or the finite version of (6) was used, as physically appropriate, at all points except when $k = M$.

To complete the solution, Eq. (21) must be discretized. This was accomplished as follows: the μ derivative of Z_s was replaced by a finite-difference approximation; the integral was approximated by a sum; and the infinite sums of index m were truncated to avoid aliasing. For $\mu_0 = M\Delta\mu$, and for N even, the result was

Unauthenticated | Downloaded 10/11/24 11:03 AM UTC

TABLE 1. Verification of numerical results by comparison of K_1 scattered sea surface elevation with analytic scattered solution for an elliptic island with incoming unit Sverdrup wave with $\theta = 90°$.

ϕ (deg)	Z_s^1: Analytic Real	Z_s^1: Analytic Imaginary	Z_s^2: Numerical Real	Z_s^2: Numerical Imaginary	Modulus of difference $\lvert Z_s^1 - Z_s^2 \rvert$
0	−0.853	−0.190	−0.846	−0.187	0.007
30	−0.843	0.335	−0.835	0.335	0.008
60	−0.611	0.785	−0.604	0.781	0.008
90	−0.202	1.028	−0.198	1.021	0.008
120	0.265	0.982	0.264	0.974	0.008
150	0.647	0.668	0.642	0.662	0.008
180	0.852	0.188	0.845	0.185	0.007
210	0.841	−0.340	0.833	−0.339	0.008
240	0.606	−0.790	0.599	−0.785	0.008
270	0.196	−1.031	0.192	−1.023	0.008
300	−0.270	−0.982	−0.269	−0.975	0.008
330	−0.649	−0.668	−0.645	−0.663	0.007

$$[3Z_s(\mu_0,l\Delta\phi) - 4Z_s(\mu_0 - \Delta\mu,l\Delta\phi) + Z_s(\mu_0 - 2\Delta\mu,l\Delta\phi)]/2\Delta\mu - \sum_{\tilde{l}=0}^{N-1}\left\{Z_s(\mu_0,l\Delta\phi)\left[\sum_{m=0}^{n}\frac{Se_m(\tilde{l}\Delta\phi)Se_m(l\Delta\phi)}{\bar{N}e_m} \times \frac{He'_m(\mu_0)}{He_m(\mu_0)} + \sum_{m=1}^{n-1}\frac{So_m(\tilde{l}\Delta\phi)So_m(l\Delta\phi)}{\bar{N}o_m} \times \frac{Ho'_m(\mu_0)}{Ho_m(\mu_0)}\right]\Delta\phi\right\} = 0, \quad (22)$$

where $n = N/2$ and $l = 0, 1, 2, \ldots, N - 1$. [The bars over Ne and No indicate that the discrete approximation of the normalization constants of (11) are to be used. The numerical values of the Mathieu functions were calculated by an algorithm given by Clemm (1969).]

This set of finite-difference equations resulted in a system of algebraic linear equations. The unknown Z_s was then numerically determined by Gaussian elimination.

6. Verification of the numerical model

The numerical results of Section 5 were compared with an analytic solution to independently verify the numerical solution. The incoming wave was defined as a unit-amplitude plane wave, the Sverdrup wave, which satisfies (5) and is written as

$$Z_0 = \exp[iK(x\cos\theta + y\sin\theta)], \quad (23)$$

where θ is the angle of incidence measured counterclockwise from the x axis. The incoming wave interacted with a cylindrical elliptic island on a flat-bottomed f-plane ocean. The analytic solution (cf. Reynolds, 1975) followed the method of McLachlen (1947), who solved the problem for $f = 0$.

Since one of the eventual goals was to model the Hawaiian Ridge, an elliptic island was used to approximately represent the ridge. For the entire ridge from Kure Island (west of Midway) to the island of Hawaii, the following parameters were assigned:

major elliptic axis: 2700 km
minor elliptic axis: 60 km
average depth: 4.5 km

f: 5.93×10^{-5} s^{-1} (at average latitude of 24° N).

The radial grid increment, $\Delta\mu = 0.22$ rad, was set equal to the μ coordinate of the ellipse representing the island; the azimuthal increment was chosen as $\Delta\phi = 6°$. The grid size was taken as 6 (μ increments) × 60 (ϕ increments).

The analytic and numerical results were compared at the main diurnal K_1 and semidiurnal M_2 tidal frequencies for a number of different values of θ. The worst results were obtained for the K_1 tidal frequency with $\theta = 90°$. The comparison of the scattered waves along the island ellipse, $\mu = \Delta\mu$, at ϕ intervals of 30°, is shown in Table 1. The results

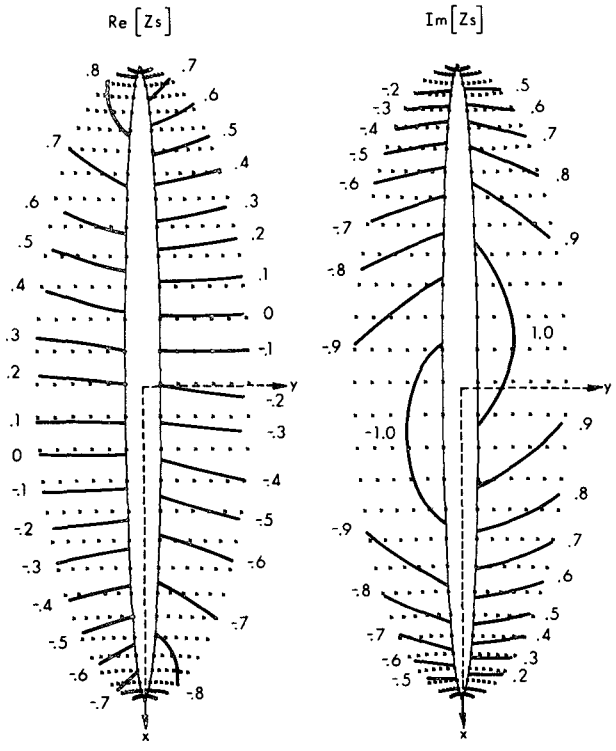

FIG. 1. Scattered sea surface elevation resulting from the interaction of an incoming K_1 tidal Sverdrup wave with an elliptic island on a flat bottom with rotation. (The grid points are indicated by dots.)

Unauthenticated | Downloaded 10/11/24 11:03 AM UTC

show that the worst relative tidal error is always less than 1% of the incoming wave amplitude.

[A numerical polar coordinate version of this program agreed to within 5% when compared with the analytic solutions for two circular islands: the flat-bottomed, f-plane solution of Proudman (1914) and the $f = 0$, radially parabolic solution of Homa (1950).]

7. Results for elliptic topographies

To demonstrate the effects of rotation and topography on the scattered wave, computations were made for the following four cases:

Figure	Model	Topography	Rotation
1	Island	Flat-bottom	$f > 0$
2	Island	Flat-bottom	$f = 0$
3	Island	Depth depends on μ	$f > 0$
4	Submerged ridge	Depth depends on μ	$f > 0$

The left portion of each figure shows the real part of the scattered wave, i.e., the scattered wave elevation at $\sigma t = 0$, the right portion shows the imaginary part, i.e., the elevation at $\sigma t = \pi/2$. The incoming wave was obtained from (23) at the K_1 tidal frequency with $\theta = 90°$. Thirty-one new grid points

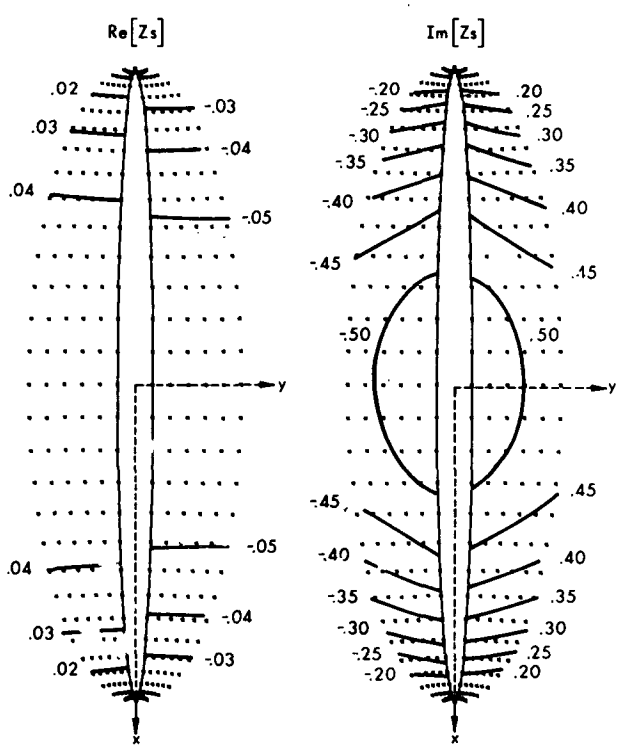

FIG. 2. Scattered sea surface elevation resulting from the interaction of an incoming K_1 tidal Sverdrup wave with an elliptic island on a flat bottom without rotation. (The grid points are indicated by dots.)

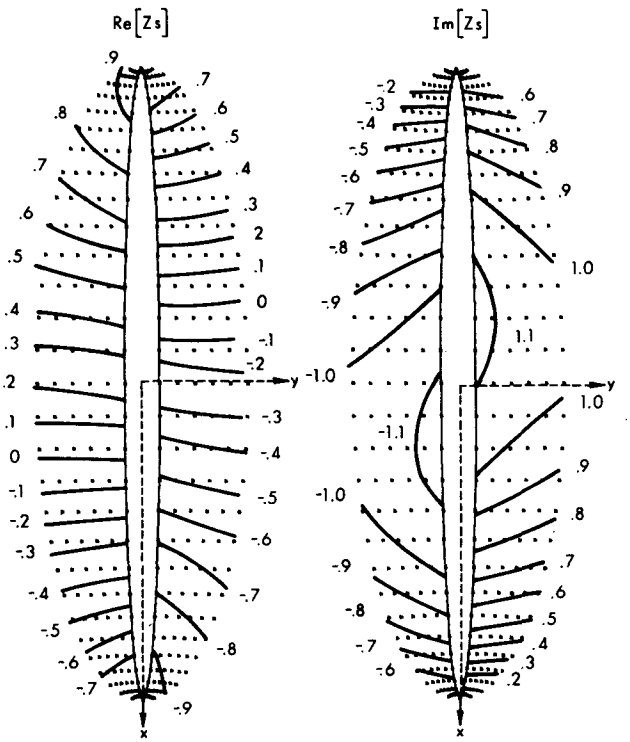

FIG. 3. Scattered sea surface elevation resulting from the interaction of an incoming K_1 tidal Sverdrup wave with an elliptic island with a radial, depth-dependent topography with rotation. (The grid points are indicated by dots.)

(at a depth of 50 m) were added to the submerged ridge model to permit flow across the island. The depth profiles for each case are shown in Fig. 5 along the y axis.

The effect of rotation can be observed by comparing the results of Figs. 1 and 2. In both cases the incoming waves and the islands were symmetric about the y axis. When the rotation was zero, the scattered wave must also be symmetric about the y axis as shown in Fig. 2. However, when $f > 0$, the flow was always deflected to the right producing the lack of symmetry which is clearly indicated in Fig. 1.

When the $\exp(-i\sigma t)$ time-dependence is restored, the scattered wave fields can be obtained for a full period of oscillation. The scattered wave with $f > 0$ can be shown to be progressive wave that moves clockwise (counterclockwise for $f < 0$) around the island. However, when $f = 0$, the scattered wave must be symmetric about the y axis and thus is reduced to a standing wave.

The effects of topography on the scattered waves are shown in Figs. 3 and 4. In the example of Fig. 3 the volume of the ridge was more than doubled (cf. Fig. 5) compared to the flat-topography case. However, there was only slight increase in the scattered wave compared to the flat-topography case of Fig. 1.

Unauthenticated | Downloaded 10/11/24 11:03 AM UTC

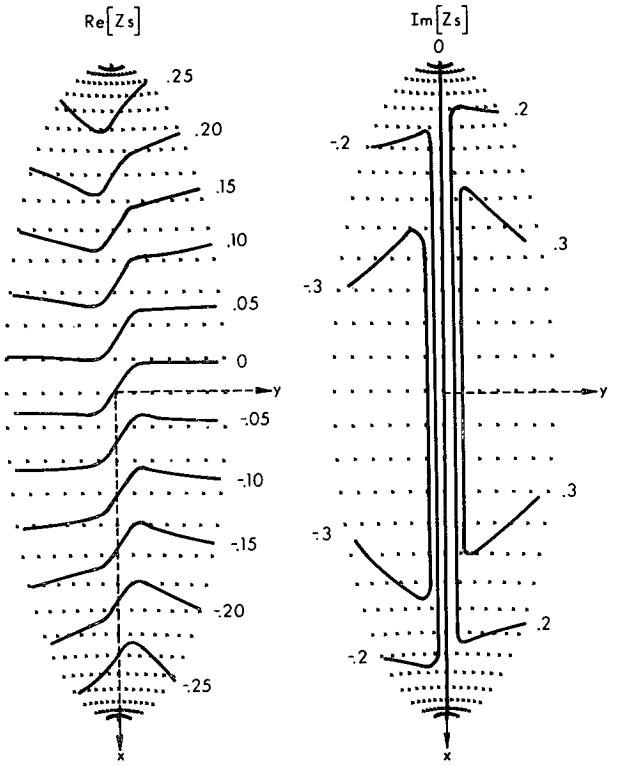

Fig. 4. Scattered sea surface elevation resulting from the interaction of an incoming K_1 tidal Sverdrup wave with a submerged elliptic ridge on a flat bottom with rotation. (The grid points are indicated by dots.)

If, however, the island was allowed to submerge to only 50 m below the sea surface (Fig. 4), the elevation of the scattered wave was considerably smaller than that shown in Fig. 1. Once water was allowed to flow across the ridge, the differences in wave elevation were quickly equalized. Thus the projection of a submarine ridge through the sea surface (to form an island) is more significant than the bathymetry adjacent to the ridge.

8. Effect of Hawaiian Ridge on the tides

To study the effect of the Hawaiian Ridge on the tides with this numerical scheme, it was necessary to determine what possible types of models could be practically treated. The first limitation was computer size. The submerged ridge model, from the preceding section, required almost all the available high-speed computer storage on the University of Hawaii IBM-360. Thus the grid scheme had to be restricted to this resolution. Unfortunately, this grid was too coarse to adequately resolve channels through the ridge and to resolve some of the major islands.

The remaining two limitations came from (22) where the sea surface elevations were computed using a truncated series expansion. If the amplitudes of the neglected higher order admittances were significant their aliasing would occur and (22) would not be a good discrete approximation for (21). Numerical tests with the present grid system have shown that these higher order admittances could be neglected if depth contours and island boundaries were along simple ellipses of constant μ.

The remaining outer boundary limitation came from the fact that (22) is valid only over a flat bottom. Since the finite difference form of the μ derivative spans the outer three μ points, the depth of the outer three ellipses must be set to the deep water constant depth h_0.

With these restrictions, three crude Hawaiian Ridge models were investigated: 1) Large Island, 2) Submerged Ridge and 3) Small Island. The Large Island model represented the ridge as an elliptic island whose major axis was equivalent to the distance between Kure Island and the island of Hawaii. The Submerged Ridge model represents the ridge as a submerged elliptic ridge whose major axis was the same as that of the foregoing Large Island. Finally, the Small Island represented the ridge as an elliptic island whose major axis was equivalent to the distance from Kauai to Hawaii.

To complete the description of these models the minor elliptic axes and the remaining depths had to be determined. To fix these parameters, 49 equally spaced cross sections of the actual ridge were used. These cross sections were then separated into those profiles which reached the surface

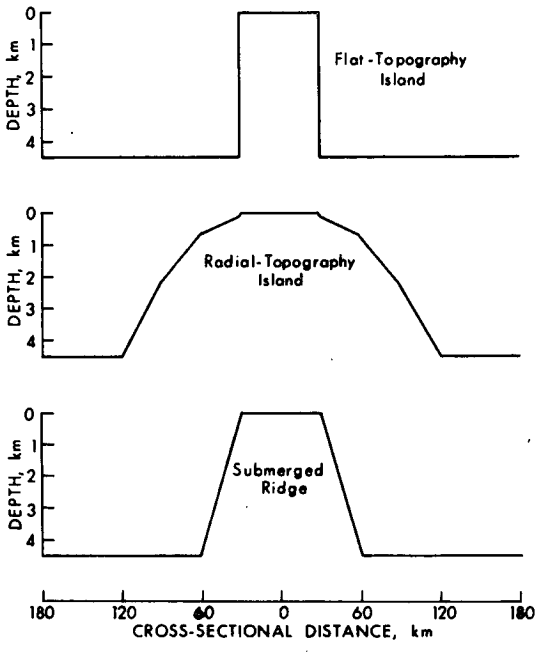

FIG. 5. Cross-sectional distance (along the y axis) for each of the topographies used in Fig. 1–4.

Unauthenticated | Downloaded 10/11/24 11:03 AM UTC

TABLE 2. NOAA tidal constants for the Hawaiian Ridge.

Station	K_1 Tide		M_2 Tide	
	Modulus (cm)	Argument (Greenwich deg)	Modulus (cm)	Argument (Greenwich deg)
Midway	7.3	−85.8	11.2	91.6
Nawiliwili	14.8	−130.7	14.8	50.0
Honolulu	14.8	−132.3	16.2	61.2
Mokuole	17.6	−123.5	15.7	16.2
Kahului	17.2	−126.3	18.1	10.8
Kawaihae	14.8	−134.0	20.8	55.1
Hilo	16.1	−126.8	21.2	31.3

and those that did not. For each class an average μ bottom depth profile was obtained; the minor elliptic axis was then adjusted so that the depth topography could be adequately resolved by the grid system. The following values were used:

Model	Large Island	Submerged Ridge	Small Island
Major axis	2700 km	2700 km	750 km
Minor axis	60 km	15 km	60 km
$\Delta\mu$	0.022 rad	0.05 rad	0.802 rad
h (0)	0 m	50 m	0 m
h (1)	50 m	50 m	50 m
h (2)	600 m	800 m	600 m
h (3)	2300 m	2300 m	2300 m
h_0	4500 m	4500 m	4500 m

In addition to the above models, a no-topography model was included. This model had neither depth-dependence nor islands. Thus, there can be no scattered wave, and the solutions were simply the incoming wave. This model was included as a check on the reasonability of the final results.

The incoming wave was constructed by a superposition of different unit amplitude discrete Sverdrup waves [Eq. (23)] at incident angles from 0° to 345° in 15° intervals. The complex amplitudes were least-squares fit to observations at seven stations for both the K_1 and M_2 tidal frequencies (cf. Table 2). If the observed amplitude at the jth station is Z_j and p is the total number of waves, then the complex amplitude, E_l, for the lth wave was obtained by minimizing Γ, where Γ is defined by

$$\Gamma = \sum_{j=1}^{7} \left| Z_j - \sum_{l=1}^{p} E_l \hat{Z}_{lj} \right|^2.$$

Here $\hat{Z}_{lj}$ is the numerically calculated total wave amplitude and was determined for each incoming wave, topography and frequency at the location of the jth station.

To select a best set of waves for each topography and frequency a residual rms error R was used which is defined as

$$R = \left(\frac{\Gamma}{\sum_{j=1}^{7} |Z_j|^2} \right)^{1/2}.$$

For each number of waves all combinations of the 24 incident directions were investigated and the result with the lowest residual was chosen as the best combination.

TABLE 3. Fitted results for each topography for incoming K_1 and M_2 Sverdrup waves.

Tidal constituent	Topographical model	Number of waves	Residual rms error (%)	First wave			Second wave		
				Incident angle (deg)	Modulus (cm)	Argument (deg)	Incident angle (deg)	Modulus (cm)	Argument (deg)
K_1	Large Island	1	47.8	−150	8.3	−108			
		2	14.0	105	55.8	145	120	58.0	−48
K_1	Submerged Ridge	1	24.0	−135	13.8	−118			
		2	12.3	105	70.3	134	120	74.7	−55
K_1	Small Island	1	36.2	120	13.6	−127			
		2	12.9	120	67.2	150	135	67.1	−44
K_1	No-topography	1	23.6	180	14.6	−116			
M_2	Large Island	1	26.7	−150	12.9	59			
		2	21.3	135	5.7	57	−120	8.9	55
M_2	Submerged Ridge	1	24.0	−120	15.3	54			
		2	15.6	−75	62.9	65	−60	52.6	−112
M_2	Small Island	1	20.0	−120	16.1	41			
		2	11.5	−120	15.0	52	−30	4.3	−20
M_2	No-topography	1	35.4	−135	16.1	62			

Unauthenticated | Downloaded 10/11/24 11:03 AM UTC

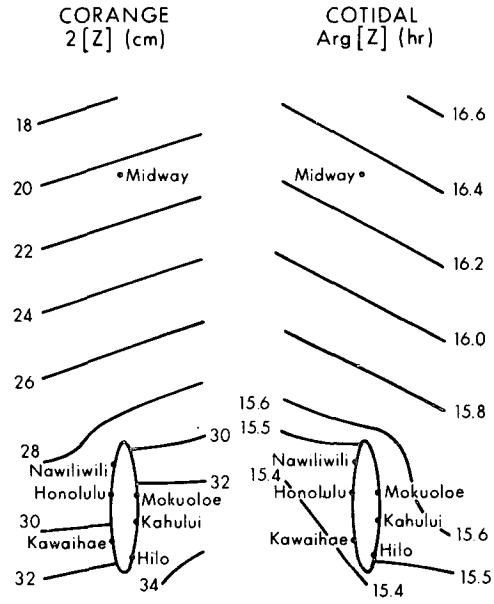

FIG. 6. Corange and cotidal chart for total fitted K_1 tide for Small Island topography with two Sverdrup waves.

The total number of waves p had to be restricted to avoid using all the available degrees of freedom. If this was not done, the resultant wave field between stations became unreasonably large. Here p was limited so that none of the individual fitted amplitudes were ever more than an order of magnitude greater than the observed station amplitude. This condition limited p to one for the no-topography model and two for the other models.

Table 3 shows the results for the different cases. The smallest residuals for the K_1 tide occurred for the two-wave Submerged Ridge model and the two-wave Small Island model. The best result for the M_2 tide was obtained from the Small Island model with two waves. Since the Small Island model was best for the M_2 tide and a close second for the K_1 tide, it might be chosen as the best of the crude approximations to the actual ridge. This would indicate that the ridge west of Kauai is unimportant in explaining the tidal distortion which has been observed in the eastern end of the Hawaiian Ridge. The best results from the Small Island model are shown in Figs. 6 and 7, which give corange and cotidal lines for the K_1 and M_2 tides. The residual error for the K_1 tide was 12.9%, and for the M_2 tide, 11.5%.

Although the residuals for the no-topography model were physically unreasonable for two waves, a comparison between the topographical models and the no-topography model can be considered if only one wave is allowed. In this particular case the smallest one-wave residuals for the M_2 tide occurred for the Small Island model. However, the smallest one-wave residual for the K_1 tide occurred for the no-topography model. The failure of the K_1 one-wave topography models to improve on the no-topography result could indicate that the topographical features which have not been included may be important.

These results should now be compared with the results of Larsen (1977). In that paper Proudman's (1914) approximate solution for a cylindrical elliptic island on an infinite flat-bottomed f-plane was used to study the tides of the Hawaiian Ridge. Although Larsen used an island similar to the Small Island model, his least square-fitting procedure was different since he included a forced tide wave and did not include the Hawaiian station at Midway. When his results were compared with the results of Figs. 6 and 7, the cotidal and corange lines were found to be of similar magnitudes but of considerably different directions. However, if the Midway tidal station were eliminated from the Small Island model's fitting procedure, and if an extra free Sverdrup wave were included to approximate the Larsen's forced wave (with direction given by the equilibrium tide as described in Larsen, 1977), the Small Island fitted results would approach Larsen's result near the island. (The remaining differences, ~10%, would be due to topographical effects, different island dimensions, etc.) The solutions in the far-field would not agree because Proudman's f-plane solution is valid only near the island. Thus the Midway tidal result could not be accurately included in Larsen's fit since Midway is located in the far-field. It is the opinion of this author that the entire ridge should be included in a tidal model of the Hawaiian Ridge since the wavelengths of the

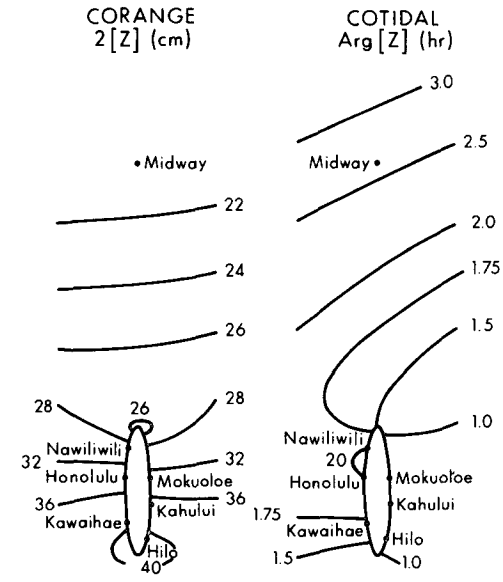

FIG. 7. Corange and cotidal chart for total fitted M_2 tide for Small Island topography with two Sverdrup waves.

Unauthenticated | Downloaded 10/11/24 11:03 AM UTC

tides are so large. In this case, the Small Island results are clearly preferable to Larsen's results.

It is important to recall that the *f*-plane ridge model presented here was very crude and that the choice of two Sverdrup waves was probably not sufficient to represent the actual incoming tidal wave field. It is also necessary to remember that most (six out of seven) of the tidal records were from stations in the eastern part of the ridge. Thus the final results can be only approximate indications of the actual tides of the Hawaiian Ridge and may have overemphasized the importance of the eastern end.

9. Summary

An open-ocean matching condition for an infinite ocean was used in a numerical model of an elliptic ridge. In this study it was found that tidal wave height was greatly modified when a submerged elliptic ridge was raised to become an island but was not greatly affected by topographical changes at depths below about 100 m. In an approximate model of the entire Hawaiian Ridge, residual rms errors of less than 15% for both K_1 and M_2 tides were presented.

Acknowledgments. The author is grateful to Brent Gallagher, Gordon Groves, Klaus Hasselmann, James Larsen, Gaylord Miller, Rudolf Preisendorfer and David Stoutemyer for their helpful comments and discussion. This work was supported by National Science Foundation under Grant GA-17137.

REFERENCES

Blanch, G., 1964: Mathieu functions. *Handbook of Mathematical Functions*, M. Abramowitz, and I. A. Stegun, Eds., *Appl. Math. Ser.*, No. 55, Nat. Bur. Stands., Washington, D.C., 1046 pp. (see pp. 721–750).

Chester, C. R., 1971: *Techniques in Partial Differential Equations*. McGraw-Hill, 440 pp.

Clemm, D. S., 1969: Algorithm 352, Characteristic values and associated solutions of Mathieu's differential equations. *Commun. ACM*, **12,** 399–407.

Hendershott, M. C., 1973: Ocean tides. *Trans. Amer. Geophys. Union*, **54,** 76–86.

——, and W. H. Munk, 1970: Tides. *Annual Reviews of Fluid Mechanics*, Vol. 2. Annual Reviews, Inc., 205–224.

Homa, S., 1950: On the behavior of seismic sea waves around circular island. *Geophys. Mag.*, **11,** 199–208.

Larsen, J. C., 1977: Cotidal charts for the Pacific Ocean near Hawaii using *f*-plane solutions, *J. Phys. Oceanogr.*, **7,** 100–109.

Luther, D. S., and C. Wunsch, 1975: Tidal charts of the central Pacific Ocean. *J. Phys. Oceanogr.*, **5,** 222–230.

McLachlan, N. W., 1947: *Theory and Application of Mathieu Functions*. Oxford University Press, 401 pp.

Morse, P. M., and H. Feshbach, 1953: *Methods of Mathematical Physics*, Vol. 2. McGraw-Hill, 1978 pp.

Platzman, G. W., 1971: Ocean tides and related waves. *Mathematical Problems in the Geophysical Sciences*, by W. H. Reid, Vol. 2, Amer. Math. Soc., 370 pp. (see pp. 239–291).

Preisendorfer, R. W., 1972: Surface wave transport in nonuniform canals. Rep. No. HIG-72-18, Hawaii Institute of Geophysics, University of Hawaii, 130 pp.

Proudman, J., 1914: Diffraction of tidal waves on flat rotating sheets of water. *Proc. London Math. Soc.*, **15,** 80–102.

Reynolds, R. W., 1975: Effects of an elliptic ridge on waves of tidal frequency. Rep. HIG-75-22, Hawaii Institute of Geophysics, University of Hawaii, 93 pp.

Unauthenticated | Downloaded 10/11/24 11:03 AM UTC